Evidence for postseismic deformation of the lower crust following the 2004 Mw6.0 Parkfield earthquake

Lucile Bruhat,[1,2] Sylvain Barbot,[1] and Jean-Philippe Avouac[1]

Received 2 November 2010; revised 22 February 2011; accepted 4 May 2011; published 5 August 2011.

[1] Previous studies have shown that postseismic relaxation following the 2004 Mw6.0 Parkfield, CA, earthquake is dominated by afterslip. However, we show that some fraction of the afterslip inferred from kinematic inversion to have occurred immediately below the seismically ruptured area may in fact be a substitute for viscous postseismic deformation of the lower crust. Using continuous GPS and synthetic aperture radar interferometry, we estimate the relative contribution of shallow afterslip (at depth less than 20km) and deeper seated deformation required to account for observed postseismic surface displacements. Exploiting the possible separation in space and time of the time series of displacements predicted from viscoelastic relaxation, we devise a linear inversion scheme that allows inverting jointly for the contribution of afterslip and viscoelastic flow as a function of time. We find that a wide range of models involving variable amounts of viscoelastic deformation can fit the observations equally well provided that they allow some fraction of deep-seated deformation (at depth larger than ~20 km). These models require that the moment released by postseismic relaxation over 5 years following the earthquake reached nearly as much as 200% of the coseismic moment. All the models show a remarkable complementarity of coseismic and shallow afterslip distributions. Some significant deformation at lower crustal depth (20–26 km) is required to fit the geodetic data. The condition that postseismic deformation cannot exceed complete relaxation places a constraint on the amount of deep seated deformation. The analysis requires an effective viscosity of at least ~10^{18} Pa s of the lower crust (assuming a semi-infinite homogeneous viscous domain). This deep-seated deformation is consistent with the depth range of tremors which also show a transient postseismic response and could explain as much as 50% of the total postseismic geodetic moment (the remaining fraction being due to afterslip at depth shallower than 20 km). Lower crustal postseismic deformation could reflect a combination of localized ductile deformation and aseismic frictional sliding.

Citation: Bruhat, L., S. Barbot, and J.-P. Avouac (2011), Evidence for postseismic deformation of the lower crust following the 2004 Mw6.0 Parkfield earthquake, *J. Geophys. Res.*, *116*, B08401, doi:10.1029/2010JB008073.

1. Introduction

[2] The 2004 Mw6.0 Parkfield, CA earthquake was a long-expected event: five Mw6.0 similar earthquakes had occurred 12 to 32 years apart since 1881 [e.g., *Bakun et al.*, 2005] at that same location but 38 years had already elapsed since the 1966 events. All these events ruptured a segment of the San Andreas fault which lies south of a 150 km long creeping segment and north of the locked Cholame segment, which last ruptured during the 1857 Mw7.9 Fort Tejon earthquake. The presence of multiple geodetic and seismic instruments surrounding the epicenter allowed detailed recording of many aspects of the earthquake cycle, including seismicity, secular deformation, coseismic rupture, and subsequent motion on and surrounding the fault [*Bakun et al.*, 2005; *Stuart and Tullis*, 1995; *Murray et al.*, 2001; *Waldhauser et al.*, 2004]. Previous studies have identified two areas of high coseismic slip [e.g., *Allmann and Shearer*, 2007] and the complementary location of coseismic slip and afterslip [*Johanson et al.*, 2006; *Johnson et al.*, 2006; *Langbein et al.*, 2006; *Murray and Langbein*, 2006; *Barbot et al.*, 2009a]. It has also been shown that afterslip must have been the dominant mechanism of postseismic relaxation [*Freed*, 2007] and that afterslip released a cumulative geodetic moment possibly as large as about three times the moment released coseismically [*Freed*, 2007; *Johanson et al.*, 2006]. While afterslip has been shown to dominate early postseismic relaxation following a number of earthquakes [e.g., *Nadeau and McEvilly*, 1999; *Reilinger et al.*, 2000; *Bürgmann et al.*, 2001, 2002; *Fialko*, 2004b; *Hsu et al.*, 2006; *Chlieh et al.*, 2007; *Barbot et al.*, 2008;

[1]Tectonics Observatory, Division of Geological and Planetary Sciences, California Institute of Technology, Pasadena, California, USA.
[2]Département des Géosciences, Ecole Normale Supérieure de Paris, Paris, France.

0148-0227/11/2010JB008073

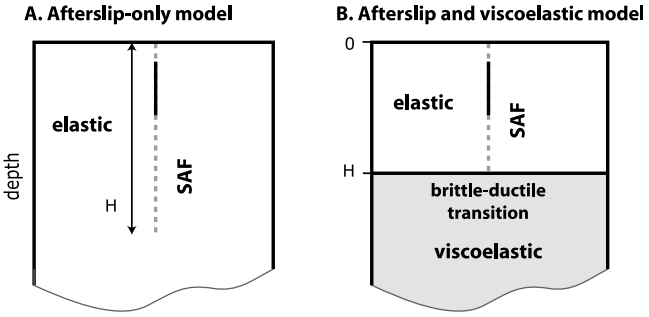

Figure 1. Model setup. (a) Postseismic deformation is modeled as resulting only from slip on a fault embedded in an elastic half-space. (b) Postseismic deformation is modeled as resulting from slip on a fault embedded in an elastic domain extending to depth H and overlying a homogeneous viscoelastic half-space.

Fielding et al., 2009; *Perfettini et al.*, 2010] this mechanism generally amounts to less than 30% of the coseismic moment. The amount of aseismic creep following the Parkfield earthquake thus seems quite exceptional.

[3] The time evolution of shallow afterslip has been found consistent with the relaxation of the coseismic stress change on portions of the fault surface with velocity-strengthening friction [*Johnson et al.*, 2006; *Barbot et al.*, 2009a]. Deep afterslip, however, seems to have evolved over a longer timescale and to increase in amplitude with depth, and is located away from areas of high coseismic slip [*Barbot et al.*, 2009a]. It is possible that the inferred deep afterslip would in fact at least partly stands for distributed viscoelastic relaxation in the lower crust. It is indeed notably difficult to discriminate localized afterslip from distributed viscous relaxation. In the case of strike slip with infinite length surface displacements induced by postseismic viscous relaxation can always been modeled as the result of some ad hoc localized slip at depth [*Thatcher*, 1983; *Savage and Prescott*, 1978] (it should be noted that the reverse is not true, however). In the case of finite length fault, the horizontal strain predicted by the two models differ only slightly at the fault tips. The two processes can however sometimes be discriminated as afterslip and viscoelastic relaxation following strike-slip earthquakes create patterns of postseismic uplift and subsidence of similar or opposite polarity depending on the depth range viscous relaxation [*Deng et al.*, 1999]. This is possible only when the vertical signature of afterslip or viscoelastic relaxation is not obscured by poroelastic effects [*Peltzer et al.*, 1996; *Fialko*, 2004a]. Despite these difficulties a number of studies have found evidence for viscoelastic relaxation, in particular following a number of other earthquakes in California [*Deng et al.*, 1998, 1999; *Freed and Bürgmann*, 2004].

[4] In this study, we estimate the extent to which postseismic surface deformation following the 2004 Parkfield earthquake reflects viscoelastic relaxation and discuss the potential bias introduced in afterslip models and its implications for the viscosity of the lower crust. The viscous properties of the lower crust around a fault zone is an important quantity to probe since it affects earthquake recurrence intervals [*Ben-Zion et al.*, 1993], the temporal variation of interseismic geodetic strain rates [*Johnson et al.*, 2007; *Perfettini and Avouac*, 2004] and stress transfer between earthquakes [*Freed and Lin*, 2001]. Compared to a previous study based on the analysis of GPS displacements recorded over 2 years after the earthquake [*Freed*, 2007], we use a more complete data set combining synthetic aperture radar (InSAR) and a 6 year long GPS time series to derive both the coseismic slip and afterslip distributions. In addition we devise and apply an inversion technique which allows us to solve jointly for coseismic slip, afterslip and postseismic viscous relaxation.

2. Evaluation of Potential Trade-Offs Between Afterslip and Viscoelastic Deformation

[5] To quantify the potential bias due to ignoring viscoelastic deformation, we use predictions of viscoelastic relaxation of horizontal surface displacements at the location of the continuous GPS stations which recorded postseismic displacements following the Parkfield earthquake and invert them for slip on the fault plane. We simulate the viscoelastic relaxation due to the stress perturbation of the 2004 event using the semianalytic approach of *Barbot et al.* [2009b] and *Barbot and Fialko* [2010a, 2010b] assuming a uniform linear viscosity in a viscoelastic half-space below $H = 20$ km depth (Figure 1b). *Ozacar and Zandt* [2009] estimate a Moho depth of ~26 km near Parkfield, so our model corresponds to viscous flow of the lower crust. We compute the stress perturbation due to the coseismic rupture based on a slip model described in section 3 using the semianalytic expressions of *Okada* [1992].

[6] The predictions of surface deformation after half a Maxwell relaxation time are shown in Figure 2a and exhibit the characteristic four quadrants of uplift and subsidence separated by two nodal planes. We reduce the synthetic GPS data using the same inversion methodology as described in section 3. As expected, the quality of fit to the horizontal viscoelastic displacement by the afterslip model is best near the fault-perpendicular nodal plane and decays near the fault tip and away from the rupture. The vertical displacements predicted by the afterslip model are anticorrelated with the vertical signal induced by postseismic relaxation showing the importance of observational constraints on vertical displacements to discriminate both models. The inferred afterslip model is shown in Figure 2b. Most slip concentrates at depth in areas of low resolution, where only large slip patches can be resolved well [*Barbot et al.*, 2009a; *Page et al.*, 2009], with an along-strike variation of amplitude that mimics the coseismic slip distribution above. We note that more far-field GPS stations are needed to increase resolution at depths greater than the seismogenic zone. As the magnitude of displacements due to viscoelastic relaxation increases with time, the amplitude of the best fitting slip model increases with postseismic time as well, with a maximum slip of 8 cm after half a Maxwell relaxation time evolving to 56 cm at complete relaxation. We do not observe a significant evolution of the spatial distribution of inferred slip, indicating that the predictions of viscoelastic displacements at the GPS stations are nearly separable in space and time. As the maximum inferred afterslip following the 2004 Parkfield event does not exceed 50 cm [e.g., *Johanson et al.*, 2006; *Barbot et al.*, 2009a] (also this study), a viscoelastic relaxation may severely bias the deep portion

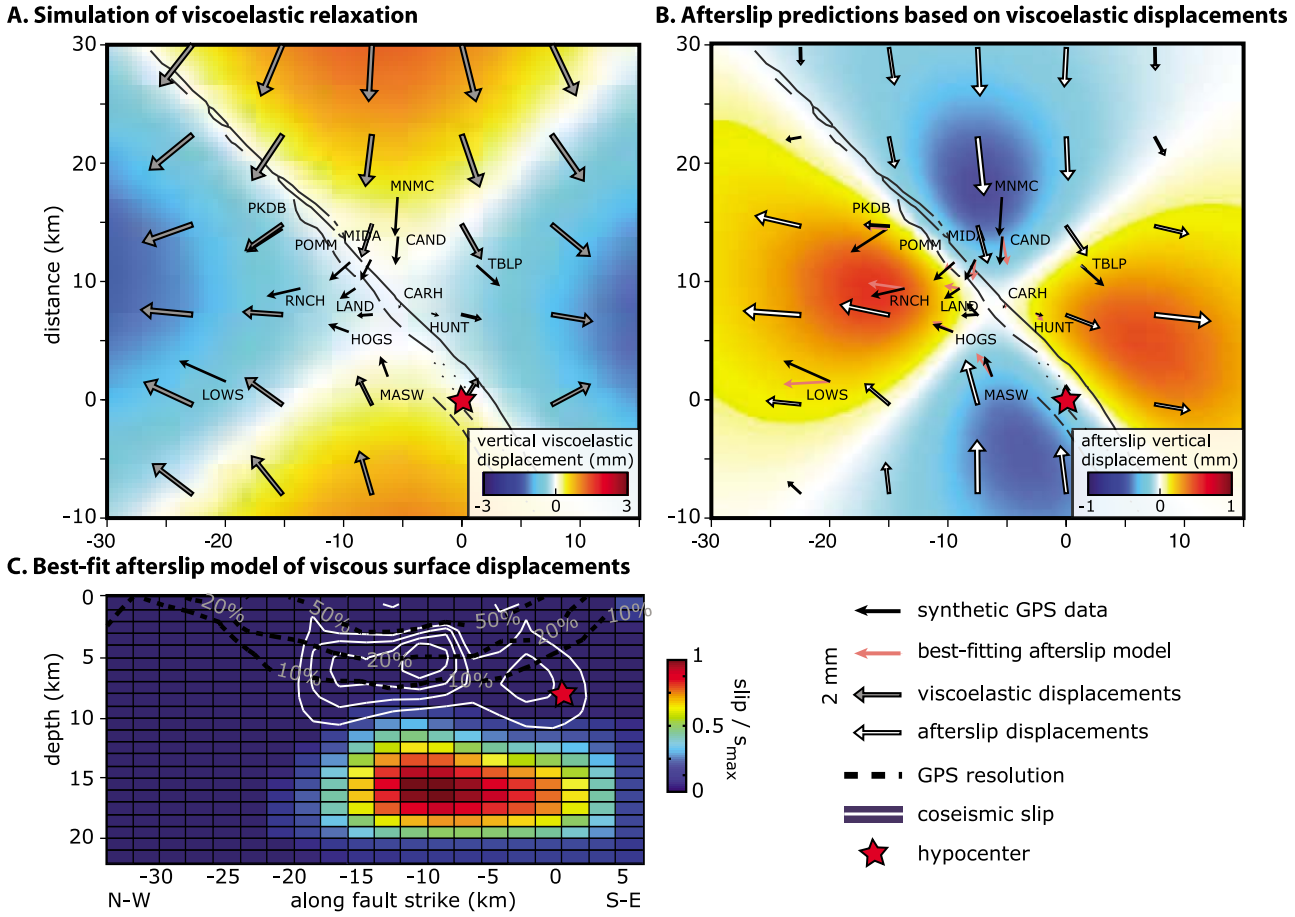

Figure 2. (a) Map view of predicted cumulative surface displacements due to viscoelastic flow below 20 km depth following the 2004 earthquake after half a Maxwell relaxation time. (b) Afterslip model best explaining the horizontal displacements predicted at the location of the GPS stations by the viscoelastic relaxation model. The amplitude of slip is time-dependent, with maximum slip $s_{max}(t_m/2) = 0.08$ m and $s_{max}(\infty) = 0.56$ m. Coseismic slip distribution (white solid lines) and areas of good resolution (dashed black contours) are shown for reference. (c) Predictions of surface displacements corresponding to the best fitting afterslip model. Note the opposite polarity of vertical displacement compared to viscoelastic deformation.

of kinematic afterslip models. The linear correlation between viscous deformation and afterslip is shown in Figure S1b and indicates that some shallow afterslip may be misplaced at greater depths if viscoelastic deformation is significant in the data and not accounted for in the modeling.[1]

3. Joint Inversion of Afterslip and Viscoelastic Relaxation

[7] We examine the coseismic and postseismic geodetic data associated with the 2004 Parkfield rupture and eventual contribution of viscoelastic relaxation, in combination to afterslip. We consider models where only afterslip is allowed (Figure 1a) and models where afterslip is allowed down to a certain depth H (which we varied between 15 and 28 km) and viscoelastic deformation is allowed at greater depth (Model B). The elastic and viscoelastic domains have the same elastic properties (G = 30 GPa, and ν = 1/4). The viscosity of the viscoelastic domain, η, is assumed uniform and isotropic. We use 14 GPS stations of the SCIGN network, continuously collecting data since 1999. We consider the daily position time series computed at the Scripps Orbit and Permanent Array Center [*Langbein and Bock*, 2004]. We determine the interseismic velocities from the slope of the displacements between the first available date and late 2003, to eliminate potential bias due to the nearby 22 December 2003 Mw 6.5 San Simeon earthquake and isolate the coseismic and postseismic signals (see Table S2). For coseismic data, we consider both horizontal and vertical offsets. For the postseismic period, however, we discard vertical GPS displacements from our analysis due to a low signal-to-noise ratio. We include five interferograms (Table S1) that were corrected for interseismic deformation assuming uniform slip rate of 32 mm/yr below 12 km by *Johanson et al.* [2006].

[8] Taking advantage of the fact that predictions of viscoelastic relaxation are separable in space and time to first

[1] Auxiliary materials are available in the HTML. doi:10.1029/2010JB008073.

order, we devise an inversion scheme that resolves quantitatively the relative contribution of afterslip on the fault and viscoelastic flow in the deeper substrate. We construct a design matrix **G** by evaluating the Green function of surface displacements due to (1) slip on each of the 300 fault patches [*Okada*, 1992] and (2) complete relaxation of coseismic deviatoric stress of the viscoelastic substrate [*Barbot and Fialko*, 2010b]. Our modeling approach is to neglect the coupling between afterslip and viscoelastic relaxation [*Johnson et al.*, 2009], and can lead to an underestimation of the viscosity in the lower crust. We refer to the vector **m** as the set of model parameters, including coseismic slip, afterslip and amplitude of viscous deformation. A 100% amplitude corresponds to complete viscous relaxation. Note that if we don't impose any bound on the amplitude of viscous deformation, the inferred postseismic deformation may be found to exceed the deformation corresponding to complete relaxation. This would be an unphysical result, except if the coseismic stress transfer has been underestimated or afterslip has contributed to a significant additional stress transfer, or the depth to the viscous layer is shallower than assumed in the model used to compute the Green functions. InSAR data span both the coseismic and postseismic periods, while the GPS data allow us to distinguish coseismic and postseismic displacements, so we solve simultaneously for coseismic slip and afterslip using the GPS and InSAR data jointly. We associate the data vector

$$\mathbf{d} = \begin{pmatrix} \mathbf{d}_{GPS}^{co} \\ \mathbf{d}_{GPS}^{post} \\ \mathbf{d}_{SAR} \end{pmatrix} \tag{1}$$

to the matrix of Green functions relating fault slip and amplitude of viscous deformation to surface deformation

$$\mathbf{G} = \begin{pmatrix} \mathbf{G}_{GPS}^{co} & 0 \\ 0 & \mathbf{G}_{GPS}^{post} \\ \mathbf{G}_{SAR}^{co} & \mathbf{G}_{SAR}^{post} \end{pmatrix}. \tag{2}$$

We estimate the contribution of afterslip and viscous relaxation by minimizing the norm $\chi = \|\mathbf{d} - \mathbf{Gm}\|$ where **d** is data vector including InSAR and GPS measurements, subjected to $\mathbf{m} \geq 0$ and the regularization

$$\mathbf{Dm} = 0. \tag{3}$$

The constraint (3) includes regularization of the coseismic slip and afterslip models (by minimization of the Laplacian) and damping of models parameters (slip on the fault North, South, and bottom boundaries and amplitude of viscoelastic deformation). The joint inversion of GPS and InSAR data allows us to discriminate coseismic and postseismic slip without making any assumption about the timescale of the postseismic transient or about the contribution of coseismic deformation in the InSAR data.

[9] The fit to the GPS and InSAR are shown in Figures 3 and 4, and the resulting afterslip models are shown in Figure 5 for two cases. Model A allows for transient afterslip only down to depth H. Figure 5a shows the afterslip models 0.02, 0.19 and 0.24 years after the main shock in the absence of viscoelastic relaxation for H = 20 km. This model shows a spatial complementarity with the coseismic model, afterslip occurring around the coseismic rupture and between the zones of high coseismic slip. It is possible that the little overlap between afterslip and coseismic slip is essentially due to the smoothing effect of the method used to regularize the inversion. The afterslip patch which lies below the coseismic rupture area becomes dominant after about 3 months (0.19 years). The inferred deep afterslip is reminiscent of the slip bias due to viscoelastic flow of Figure 2. When we allow for viscoelastic relaxation below 20 km in our inversions (with no bound on its intensity), we obtain dramatically different afterslip models, with deep afterslip being no more required and most slip concentrating at shallow depth, above the coseismic rupture (Figure 5b). The fit to the postseismic data for the afterslip only and afterslip/viscoelastic models are compared in Figures 3 and 4 for GPS and InSAR, respectively. Despite an already excellent fit of the simpler afterslip models, the fit to the geodetic data is improved when including the effect of a viscoelastic relaxation for both GPS and InSAR and for all times considered (Figures 3 and 4). The null hypothesis that the viscoelastic model with unbounded intensity does not provide a significantly better fit than the afterslip-only model is rejected within a 99% confidence using an F test, considering an increase from 300 to 301 model parameters to explain about 1500 data points including GPS and InSAR. The statistics indicates that the source of deformation at depth deeper than 20 km, represented here by viscoelastic relaxation, is not only compatible with, but also required by the geodetic data. However, the resolution of the viscous parameter in the kinematic inversion is ~60% (see Figure S1), indicating a trade-off with other mechanisms of deformation that cannot be resolved automatically by the standard inversion method (see also Figure S1b). Note that the contribution of deep viscoelastic relaxation could be equally well represented by some distribution of afterslip at depth deeper than about 20 km. As H is increased, we obtain afterslip-only models in which the deep zone of afterslip extends deeper and an improved variance reduction. For H = 26 km we obtain an afterslip model with a variance reduction about as good as what can be obtained with viscoelastic relaxation at depth below 20 km (see Table 1). The viscoelastic model is more economic in terms of the number of parameters involved. Also it can be tested a posteriori since, as the evolution of viscoelastic strain is separable in space and time, the time evolution of the amplitude of the viscoelastic response should increase as $[1 - \exp(-t/t_m)]$, where $t_m = \eta/G$ is the Maxwell time.

[10] Figure 5 shows the model obtained if the contribution of viscous relaxation is left unbounded. In this model the patch of afterslip immediately below the coseismic rupture has nearly entirely disappeared suggesting it might have stand as a substitute for viscoelastic relaxation. However, this particular model implies a viscous amplitude reaching, after 5 years of postseismic relaxation, as much as three times the value predicted for complete relaxation. This model thus turns out to be unphysical. However, it indicates that the data are better adjusted if transient postseismic deformation deeper than 20 km is allowed. It could be that we have underestimated the stress changes driving postseismic deformation at depth or the effect of reloading by afterslip (deep afterslip in that case represent about 30% of the total coseismic moment). Alternatively the contribution

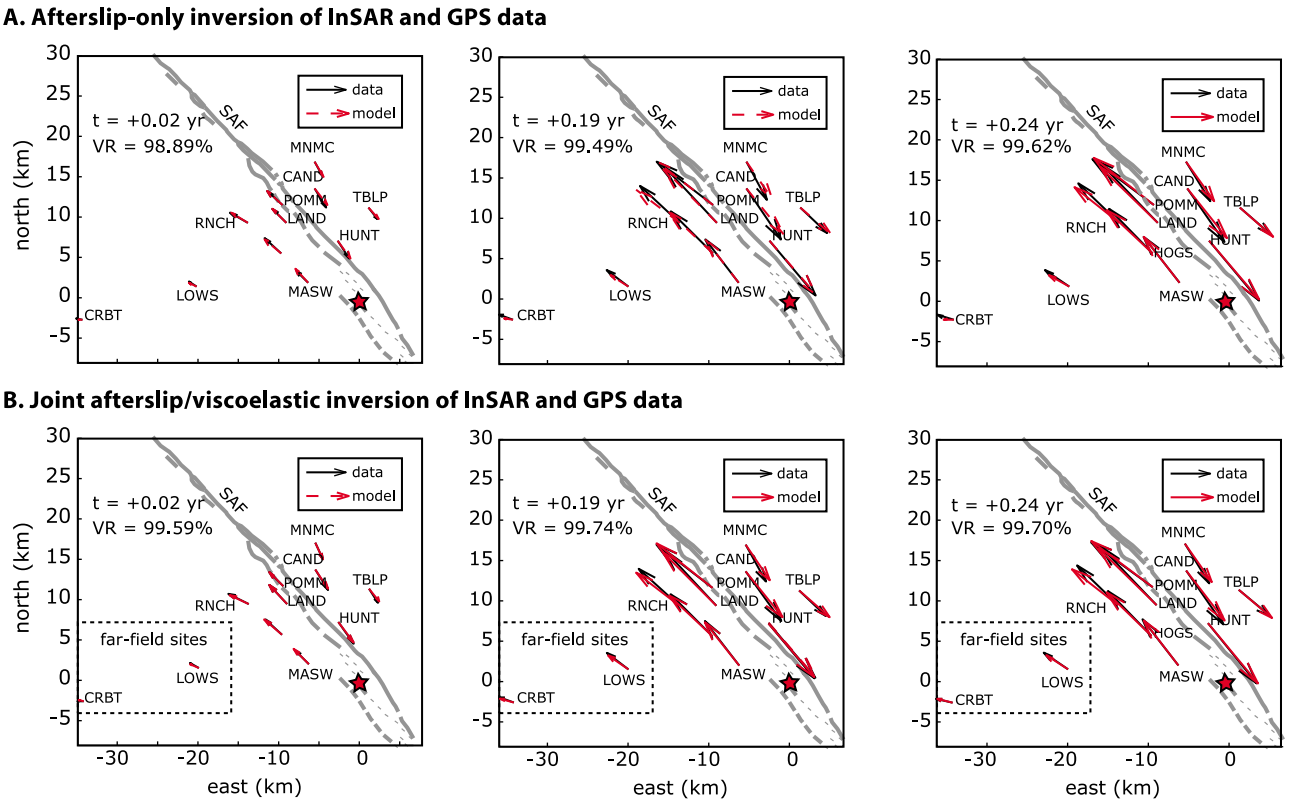

Figure 3. Comparison of the fit to the cumulative GPS displacements at various postseismic epochs for the elastic crust and the low-viscosity crust models. The inversion includes a fit to both GPS and InSAR data. Despite an excellent variance reduction (VR) of the pure afterslip models, the quality of fit is improved when accounting for a viscoelastic relaxation. The best fitting model requires three times more amplitude of viscous flow 5 years after the main shock than the one corresponding to full relaxation of a semi-infinite layer below 20 km depth. This model is only marginally better than our preferred model in which the amplitude of viscoelastic relaxation is forced to reach full relaxation at the end of the study period.

of viscous deformation may be overestimated in this inversion. We determine models with lesser amount of viscous deformation by damping the amplitude of viscoelastic deformation in our inversions. The corresponding family of afterslip models is shown in Figure S2.

[11] We test further the viscoelastic contribution by considering the time evolution of the inferred viscous deformation. We expect the amplitude of the viscous contribution in our inversions to increase monotonously with time following an exponentially decaying velocity. To resolve the time evolution of the viscous flow we use the GPS data only and invert the postseismic horizontal displacement time series from 2004 to 2010 for afterslip and viscous flow as a function of time. The time evolution of the amplitude of viscous deformation is shown in Figure 6 for two different values of damping of the viscous amplitude. In both cases we find a time evolution consistent with the response of a linear viscoelastic material indicating that a stress-dependent (non-Newtonian) viscosity, although not ruled out, is not required to explain the time evolution of GPS data if afterslip is allowed. The relaxation time of $t_m = 1.1$ years seems independent of the depth H to the viscoelastic domain and implies an effective viscosity of about $\eta = 10^{18}$ Pa s using a shear modulus of $G = 30$ GPa. Assuming a uniform depth of 20 km to the viscous medium, one can determine the minimum value of damping to bound the amplitude of viscous deformation to 100% after 5 years of postseismic relaxation (green profile in Figure 6). The corresponding afterslip model is shown in Figure 7 and implies a reduction of about 50% of afterslip compared to the afterslip-only model (from a cumulative geodetic moment of 1.5 10^{18} Nm to 8.5 10^{17} Nm). In order to assess the effect of the underlying viscosity structure, we repeat the procedure for a uniform transition depth to viscoelasticity of $H = 15$ km and $H = 30$ km. The effect of a shallower depth to the viscoelastic domain is to decrease by ~10% the moment of afterslip required to fit the data. We note that models of viscoelastic relaxation with an overriding elastic plate thicker than $H = 30$ km give rise to negligible surface deformation: So when $H > 30$ km models A and B of Figure 1 are equivalent.

4. Discussion

[12] Our analysis yields a refined coseismic slip model and a suite of possible afterslip models each of which include variable amounts of viscous relaxation. The coseismic slip model corresponds to a total moment of 1.95 10^{18} (assuming a shear modulus of $G = 30$ GPa), which implies a

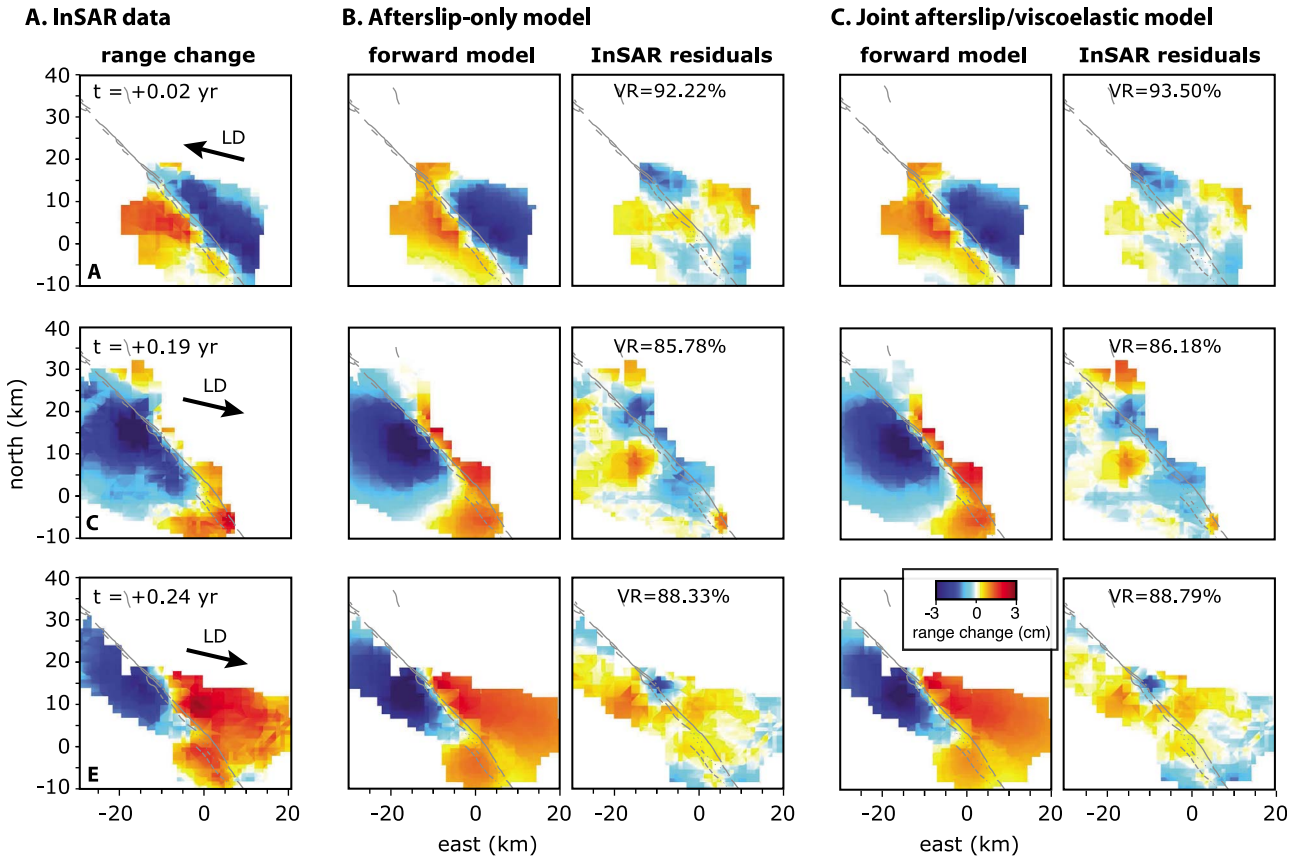

Figure 4. Comparison of the fits to the InSAR line-of-sight displacements at various postseismic epochs for the elastic crust and the low-viscosity crust models. (a) SAR interferograms 051904-100604, 082604-120904, and 061904-122804. The inversion includes a fit to both GPS and InSAR data. Fit and residuals of the (b) afterslip-only and (c) afterslip/viscoelastic model. The variance reduction is systematically improved by accounting for a viscoelastic relaxation.

moment magnitude of Mw6.0 consistent with the seismological estimate. All the models show a remarkable complementarity of coseismic slip and afterslip distributions. So this finding is a robust inference. The geodetic data require that postseismic deformation released a moment of 3.7 10^{18} Nm representing as much as 190% of the coseismic moment. So the 2004 Parkfield earthquake was followed by an exceptionally large transient postseismic deformation. Shallow afterslip explains most of the observed geodetic strain seen in the near field (at distances less than the ~15 km ruptured length, for example at GPS station *hogs* in Figure 8). The dominant fault-parallel component of shear seen in these data clearly indicates a dominant contribution of afterslip. The presence of this shallow zone, with presumably rate-strengthening friction given the approximately logarithmic time evolution of slip, is consistent with the observation of shallow aseismic creep during the interseismic and postseismic periods [*Murray et al.*, 2001; *Fialko et al.*, 2005; *Murray and Langbein*, 2006]. Our study thus confirms previous results (see reference therein) showing that the Parkfield earthquake triggered an exceptionally large amount of aseismic slip, probably due to its proximity to the creeping segment of the San Andreas Fault. However, if afterslip is limited to a 0–20 km depth range it can only account of about 80% of the displacements observed at the stations farther away from the fault (for example station *lows* in Figure 8). The deeper component of deformation is required to explain as much as 20% of the postseismic displacement at that station 5 years after the earthquake. This view is consistent with the observations of seismic tremors in the lower crust below Parkfield segment and their transient response to the 2004 earthquake [*Shelly*, 2010; *Shelly and Hardebeck*, 2010]. The amount of viscoelastic deformation is difficult to determine precisely given the trade-off between deep afterslip and viscous relaxation in the absence of good constraints on vertical displacements or on horizontal deformation near the tip of the rupture. With the constraint that viscous deformation cannot exceed that

Table 1. Variance Reduction (VR) of InSAR and GPS Data at t = 0.24 Years for the Afterslip Models and the Joint Afterslip/Viscoelastic Flow Model

Viscoelastic Flow	H (km)	GPS VR (%)	InSAR VR (%)
0% (no flow)	15	99.51	88.49
0% (no flow)	20	99.62	88.33
0% (no flow)	28	99.64	88.27
100% (relaxed)	20	99.69	88.84
300% (over-relaxed)	20	99.70	88.79
300% (over-relaxed)	28	99.70	88.81

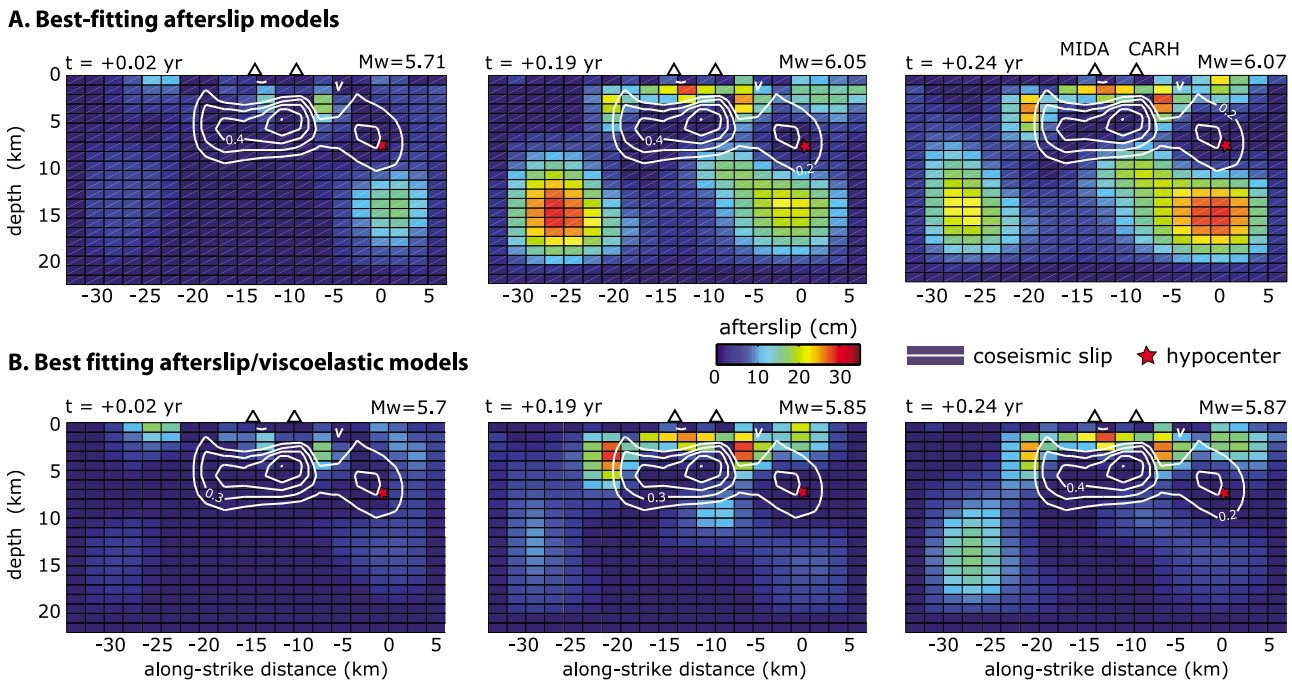

Figure 5. Afterslip derived from the joint inversion of the GPS and InSAR data for coseismic slip and afterslip 0.02, 0.19, and 0.24 years after the 2004 earthquake. We allow (a) for afterslip only or (b) for a combination of afterslip and viscous deformation below the seismogenic zone. The coseismic slip model is represented by white contour in all plots. Models in Figure 5b require an amplitude of viscous deformation three times greater than the one corresponding to the relaxation of a semi-infinite substrate below 20 km depth.

predicted for complete relaxation, and assuming that the viscoelastic domain lies at depth greater than 20 km, we get that afterslip released a geodetic moment of 1.57 10^{18} Nm representing about 80% of the coseismic moment, so that about 40% the deep afterslip geodetic moment needed to account for the 5 year postseismic transient deformation would be due to viscoelastic relaxation. Viscous relaxation could thus explain some of the measured postseismic displacements over the 6 years following the earthquake and that the effective Newtonian viscosity is not lower than 10^{18} Pa s.

[13] The deep-seated postseismic deformation could reflect either that a domain with rate-strengthening sliding extends at depth to near the Moho depth (Model A with $H \sim 26$ km) or represent the transition to more distributed viscous-like deformation in the lower crust (Model B with $H = 15 - 20$ km). The depth range of this deep deformation is consistent with the depth range of the tremors whose

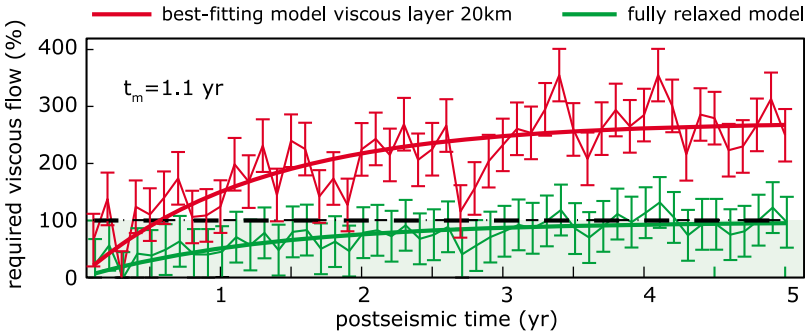

Figure 6. Evolution of the amplitude of viscoelastic deformation as a function of time after the 2004 earthquake, in proportion to the deformation corresponding to complete viscous relaxation. The depth to the viscous layer is set to 20km. The red symbols show the results obtained when the amplitude of viscous deformation in time is not bounded. This model implies a viscous component amounting to 300% of the deformation predicted for complete relaxation. The green symbols show the results obtained when the amplitude of viscous deformation is bounded to 100%, corresponding to the afterslip model in Figure 7b. The thick solid lines are a best fit with $[1 - \exp(-t/t_m)]$ with an inferred timescale of $t_m = 1.1$ years. The dashed line is the maximum allowed.

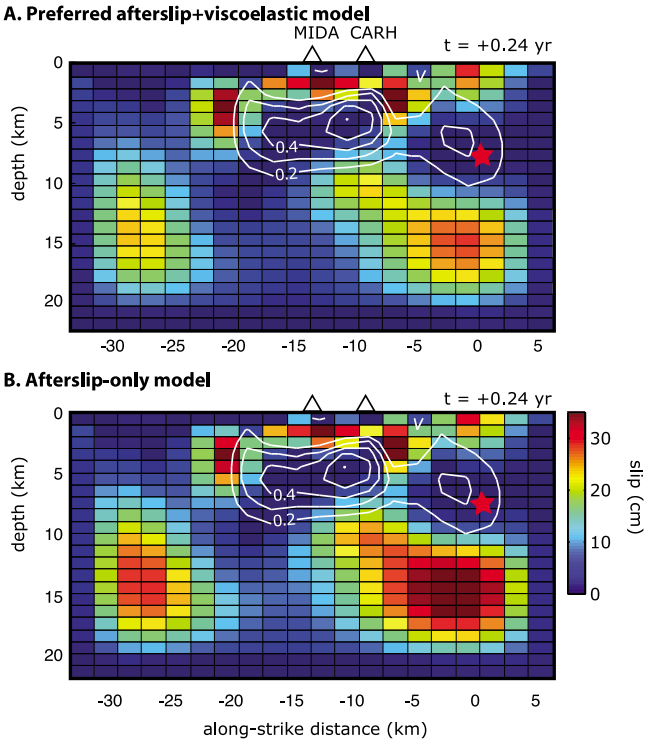

Figure 7. (a) Preferred viscoelastic + afterslip model implying fully relaxed viscoelastic flow in the lower crust accompanied by deep afterslip on the plate interface. The contour of coseismic slip distribution is shown in white. (b) Afterslip-only model showing more afterslip at depth away from the maximum coseismic stress perturbation. Moment M and moment magnitude Mw correspond to the total geodetic moment of afterslip.

activity was enhanced during postseismic relaxation. However, we note that the pattern of postseismic strain implied by Model B is more distributed than the narrow zone of tremors activity (Figure 8). The tremors distribution thus suggests a much more localized postseismic transient deformation. This could suggest that Model A is actually more appropriate and that rate-strengthening frictional sliding would be the dominant mode of deformation in the lower crust, or that ductile deformation is actually much more localized than is estimated when a homogeneous Newtonian viscosity is assumed. Strain localization of ductile deformation could be due to the effect of shear heating on the local viscosity [*Thatcher and England*, 1998; *Rolandone and Jaupart*, 2002] to the nonlinear viscous deformation or to grain-size reduction, mineral growth and reorientation in the ductile shear zone [*Gueydan et al.*, 2001, 2003; *Kelemen and Hirth*, 2007; *Landuyt and Bercovici*, 2009]. If viscoelastic flow is indeed occurring at tremogenic depth, it would imply simultaneous ductile and brittle deformation in a mixed-lithology fault zone exhibiting various degrees of localization, as is observed, for example, in mélange shear zones [*Fagereng and Sibson*, 2010].

[14] The evidence for transient deformation of the lower crust has important implications for the earthquake cycle. On the one hand, stress perturbations from the coseismic rupture may be dissipated in a viscous layer during the postseismic period. On the other hand, the loading of the seismogenic zone might differ depending on whether it is loaded from the far field or loaded from below due to flow in the lower crust and upper mantle. For instance the delayed occurrence of the 2004 Parkfield event is consistent with a decaying viscoelastic stress transfer from the 1857 Fort Tejon earthquake [*Ben-Zion et al.*, 1993]. The presence of a weak lower crust below the San Andreas Fault near Parkfield may affect stress transfer between earthquakes and should be an important element of mechanical models of stress evolution in California [e.g., *Chéry et al.*, 2001].

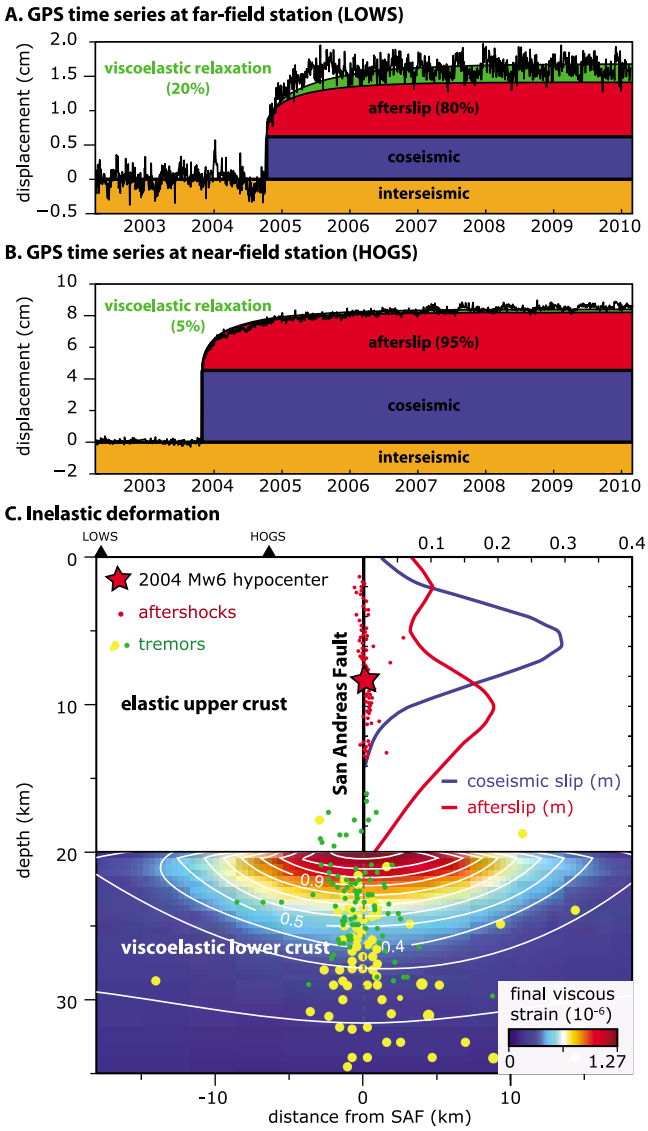

Figure 8. Relative contribution of afterslip and viscoelastic flow for (a) near-field and (b) far-field GPS stations. (c) Depth-averaged coseismic slip and afterslip and cumulative viscous strain $\gamma(\mathbf{x}) = \int_0^\infty \|\dot{\boldsymbol{\epsilon}}^i(\mathbf{x}, t')\| dt'$ in the viscoelastic substrate across the fault. The integrated strain corresponds to 2 cm of viscous displacement across the fault distributed over 20 km. The relocated catalog of aftershocks is from *Bakun et al.* [2005]. The tremor catalogs are from *Shelly and Hardebeck* [2010] (green circles) and *Ryberg et al.* [2010] (yellow circles).

[15] **Acknowledgments.** We thank I. Johanson for providing us with processed InSAR data. We are grateful for the thoughtful reviews of Roland Bürgmann and Wayne Thatcher and the comments from Editor Tom Parsons. This study was supported in part by the Gordon and Betty Moore Foundation. This is Caltech Tectonics Observatory contribution 147.

References

Allmann, B. P., and P. M. Shearer (2007), A high-frequency secondary event during the 2004 Parkfield earthquake, *Science*, *318*(5854), 1279–1283.

Bakun, W. H., et al. (2005), Implications for prediction and hazard assessment from the 2004 Parkfield earthquake, *Nature*, *437*, 969–974.

Barbot, S., and Y. Fialko (2010a), Fourier-domain Green's function for an elastic semi-infinite solid under gravity, with applications to earthquake and volcano deformation, *Geophys. J. Int.*, *182*, 568–582, doi:10.1111/j.1365-246X.2010.04655.x.

Barbot, S., and Y. Fialko (2010b), A unified continuum representation of post-seismic relaxation mechanisms: Semi-analytic models of afterslip, poroelastic rebound and viscoelastic flow, *Geophys. J. Int.*, *182*, 1124–1140, doi:10.1111/j.1365-246X.2010.04678.x.

Barbot, S., Y. Hamiel, and Y. Fialko (2008), Space geodetic investigation of the coseismic and postseismic deformation due to the 2003 M_w7.2 Altai earthquake: Implications for the local lithospheric rheology, *J. Geophys. Res.*, *113*, B03403, doi:10.1029/2007JB005063.

Barbot, S., Y. Fialko, and Y. Bock (2009a), Postseismic deformation due to the M_w 6.0 2004 Parkfield earthquake: Stress-driven creep on a fault with spatially variable rate-and-state friction parameters, *J. Geophys. Res.*, *114*, B07405, doi:10.1029/2008JB005748.

Barbot, S., Y. Fialko, and D. Sandwell (2009b), Three-dimensional models of elasto-static deformation in heterogeneous media, with applications to the eastern California Shear Zone, *Geophys. J. Int.*, *179*, 500–520.

Ben-Zion, Y., J. R. Rice, and R. Dmowska (1993), Interaction of the San Andreas Fault creeping segment with adjacent great rupture zones and earthquake recurrence at Parkfield, *J. Geophys. Res.*, *98*(B2), 2135–2144, doi:10.1029/92JB02154.

Bürgmann, R., M. G. Kogan, V. E. Levin, C. H. Scholz, R. W. King, and G. M. Steblov (2001), Rapid aseismic moment release following the 5 December, 1997 Kronotsky, Kamchatka, earthquake, *Geophys. Res. Lett.*, *28*, 1331–1334.

Bürgmann, R., S. Ergintav, P. Segall, E. H. Hearn, S. McClusky, R. E. Reilinger, H. Woith, and J. Zschau (2002), Time-dependent distributed afterslip on and deep below the Izmit earthquake rupture, *Bull. Seismol. Soc. Am.*, *92*(1), 126–137.

Chéry, J., M. D. Zoback, and R. Hassani (2001), An integrated mechanical model of the San Andreas Fault in central and northern California, *J. Geophys. Res.*, *106*(B10), 22,051–22,066.

Chlieh, M., et al. (2007), Coseismic slip and afterslip of the great Mw 9.15 Sumatra-Andaman earthquake of 2004, *Bull. Seismol. Soc. Am.*, *97*(1A), S152–S173, doi:10.1785/0120050631.

Deng, J., M. Gurnis, H. Kanamori, and E. Hauksson (1998), Viscoelastic flow in the lower crust after the 1992 Landers California, earthquake, *Science*, *282*(5394), 1689–1692.

Deng, J., K. Hudnut, M. Gurnis, and E. Hauksson (1999), Stress loading from viscous flow in the lower crust and triggering of aftershocks following the 1994 Northridge California, earthquake, *Geophys. Res. Lett.*, *26*, 3209–3212.

Fagereng, A., and R. H. Sibson (2010), Mélange rheology and seismic style, *Geology*, *38*(8), 751–754, doi:10.1130/G30868.1.

Fialko, Y. (2004a), Probing the mechanical properties of seismically active crust with space geodesy: Study of the coseismic deformation due to the 1992 M_w7.3 Landers (Southern California) earthquake, *J. Geophys. Res.*, *109*, B03307, doi:10.1029/2003JB002756.

Fialko, Y. (2004b), Evidence of fluid-filled upper crust from observations of postseismic deformation due to the 1992 M_w7.3 Landers earthquake, *J. Geophys. Res.*, *109*, B08401, doi:10.1029/2004JB002985.

Fialko, Y., D. Sandwell, M. Simons, and P. Rosen (2005), Three-dimensional deformation caused by the Bam, Iran, earthquake and the origin of shallow slip deficit, *Nature*, *435*, 295–299.

Fielding, E. J., P. R. Lundgren, R. Bürgmann, and G. J. Funning (2009), Shallow fault-zone dilatancy recovery after the 2003 Bam earthquake in Iran, *Nature*, *458*, 64–68.

Freed, A. M. (2007), Afterslip (and only afterslip) following the 2004 Parkfield, California, earthquake, *Geophys. Res. Lett.*, *34*, L06312, doi:10.1029/2006GL029155.

Freed, A. M., and R. Bürgmann (2004), Evidence of power-law flow in the Mojave Desert mantle, *Nature*, *430*, 548–551.

Freed, A. M., and J. Lin (2001), Delayed triggering of the 1999 Hector Mine earthquake by viscoelastic stress transfer, *Nature*, *441*, 180–183.

Gueydan, F., Y. M. Leroy, and L. Jolivet (2001), Grain-size-sensitive flow and shear-stress enhancement at the brittle-ductile transition of the continental crust, *J. Geophys. Res.*, *90*(1), 181–196.

Gueydan, F., Y. M. Leroy, L. Jolivet, and P. Agard (2003), Analysis of continental midcrustal strain localization induced by microfracturing and reaction-softening, *J. Geophys. Res.*, *108*(B2), 2064, doi:10.1029/2001JB000611.

Hsu, Y.-J., M. Simons, J.-P. Avouac, J. Galetzka, K. Sieh, M. Chlieh, D. Natawidjaja, L. Prawirodirdjo, and Y. Bock (2006), Friction afterslip following the 2005 Nias-Simeulue earthquake, Sumatra, *Science*, *312*(5782), 1921–1926.

Johanson, I. A., E. J. Fielding, F. Rolandone, and R. Bürgmann (2006), Coseismic and postseismic slip of the 2004 Parkfield earthquake from space-geodetic data, *Bull. Seismol. Soc. Am.*, *96*(4B), S269–S282.

Johnson, K. J., R. Bürgmann, and K. Larson (2006), Frictional properties on the San Andreas Fault near Parkfield, California, inferred from models of afterslip following the 2004 earthquake, *Bull. Seismol. Soc. Am.*, *96*(4B), S321–S338.

Johnson, K. M., G. E. Hilley, and R. Bürgmann (2007), Influence of lithosphere viscosity structure on estimates of fault slip rate in the Mojave region of the San Andreas Fault system, *J. Geophys. Res.*, *112*, B07408, doi:10.1029/2006JB004842.

Johnson, K. M., R. Bürgmann, and J. T. Freymueller (2009), Coupled afterslip and viscoelastic flow following the 2002 Denali Fault, Alaska earthquake, *Geophys. J. Int.*, *176*, 670–682.

Kelemen, P. B., and G. Hirth (2007), A periodic shear-heating mechanism for intermediate-depth earthquakes in the mantle, *Nature*, *446*, 787–790.

Landuyt, W., and D. Bercovici (2009), Formation and structure of lithospheric shear zones with damage, *Phys. Earth Planet. Inter.*, *175*(3–4), 115–126.

Langbein, J., and Y. Bock (2004), High-rate real-time GPS network at Parkfield: Utility for detecting fault slip and seismic displacements, *Geophys. Res. Lett.*, *31*, L15S20, doi:10.1029/2003GL019408.

Langbein, J., J. R. Murray, and H. A. Snyder (2006), Coseismic and initial postseismic deformation from the 2004 Parkfield, California, earthquake, observed by global positioning system, electronic distance meter, creepmeters, and borehole strainmeters, *Bull. Seismol. Soc. Am.*, *96*(4B), S304–S320.

Murray, J., and J. Langbein (2006), Slip on the San Andreas Fault at Parkfield, California, over two earthquake cycles, and the implications for seismic hazard, *Bull. Seismol. Soc. Am.*, *96*(4B), S283–S303.

Murray, J. R., P. Segall, P. Cervelli, W. Prescott, and J. Svarc (2001), Inversion of GPS data for spatially variable slip-rate on the San Andreas Fault near Parkfield, CA, *Geophys. Res. Lett.*, *28*, 359–362.

Nadeau, R. M., and T. V. McEvilly (1999), Fault slip rates at depth from recurrence intervals of repeating microearthquakes, *Science*, *285*(5428), 718–721.

Okada, Y. (1992), Internal deformation due to shear and tensile faults in a half-space, *Bull. Seismol. Soc. Am.*, *82*(2), 1018–1040.

Ozacar, A. A., and G. Zandt (2009), Crustal structure and seismic anisotropy near the San Andreas Fault at ParkÞeld, California, *Geophys. J. Int.*, *178*, 1098–1104.

Page, M. T., S. Custódio, R. J. Archuleta, and J. M. Carlson (2009), Constraining earthquake source inversions with GPS data: 1. Resolution-based removal of artifacts, *J. Geophys. Res.*, *114*, B01314, doi:10.1029/2007JB005449.

Peltzer, G., P. Rosen, F. Rogez, and K. Hudnut (1996), Postseismic rebound in fault step-overs caused by pore fluid flow, *Science*, *273*(5279), 1202–1204, doi:10.1126/science.273.5279.1202.

Perfettini, H., and J.-P. Avouac (2004), Stress transfer and strain rate variations during the seismic cycle, *J. Geophys. Res.*, *109*, B06402, doi:10.1029/2003JB002917.

Perfettini, H., et al. (2010), Seismic and aseismic slip on the central Peru megathrust, *Nature*, *465*, 78–81, doi:10.1038/nature09062.

Reilinger, R. E., et al. (2000), Coseismic and postseismic fault slip for the 17 August 1999, M = 7.5, Izmit, Turkey earthquake, *Science*, *289*(5484), 1519–1524, doi:10.1126/science.289.5484.1519.

Rolandone, F., and C. Jaupart (2002), The distributions of slip rate and ductile deformation in a strike-slip shear zone, *Geophys. J. Int.*, *148*, 179–192.

Ryberg, T., C. Harberland, G. S. Fuis, W. L. Ellsworth, and D. R. Shelly (2010), Locating non-volcanic tremor along the San Andreas Fault using a multiple array source imaging technique, *Geophys. J. Int.*, *183*, 1485–1500.

Savage, J. C., and W. H. Prescott (1978), Asthenosphere readjustment and the earthquake cycle, *J. Geophys. Res.*, *83*(B7), 3369–3376.

Shelly, D. R. (2010), Migrating tremors illuminate complex deformation beneath the seismogenic San Andreas Fault, *Nature*, *463*, 648–652, doi:10.1038/nature08755.

Shelly, D. R., and J. L. Hardebeck (2010), Precise tremor source locations and amplitude variations along the lower-crustal central San Andreas Fault, *Geophys. Res. Lett.*, *37*, L14301, doi:10.1029/2010GL043672.

Stuart, W. D., and T. E. Tullis (1995), Fault model for preseismic deformation at Parkfield, California, *J. Geophys. Res.*, *100*(B12), 24,079–24,099.

Thatcher, W. (1983), Nonlinear strain buildup and the earthquake cycle on the San Andreas fault, *J. Geophys. Res.*, *88*(B7), 5893–-5902.

Thatcher, W., and P. C. England (1998), Ductile shear zones beneath strike-slip faults: Implications for the thermomechanics of the San Andreas Fault zone, *J. Geophys. Res.*, *103*(B1), 891–905.

Waldhauser, F., W. L. Ellsworth, D. P. Schaff, and A. Cole (2004), Streaks, multiplets, and holes: High-resolution spatio-temporal behavior of Parkfield seismicity, *Geophys. Res. Lett.*, *31*, L18608, doi:10.1029/2004GL020649.

J.-P. Avouac, S. Barbot, and L. Bruhat, Tectonics Observatory, Division of Geological and Planetary Sciences, California Institute of Technology, 1200 E. California Blvd., Pasadena, CA 91125, USA. (sbarbot@caltech.edu)